

Crystal structure of double-collapsed-phase $\text{Bi}_{6+x}\text{Sr}_{9-x}\text{Fe}_5\text{O}_{26}$ and its relation to modulated-phase $\text{Bi}_2\text{Sr}_2\text{CaCu}_2\text{O}_{8+\delta}$

O. Pérez, H. Leligny, G. Baldinozzi, D. Grebille, M. Hervieu, Ph. Labbé, and D. Groult
Laboratoire CRISMAT (UMR CNRS 6508), ISMRA, 6 Bd du Maréchal Juin, 14050 Caen Cedex, France

H. Graafsma

European Synchrotron Radiation Facility, 38043 Grenoble Cedex, France

(Received 30 October 1996)

A structural analysis of the double-collapsed-phase $\text{Bi}_{6+x}\text{Sr}_{9-x}\text{Fe}_5\text{O}_{26}$ is presented in light of the modulated-phase $\text{Bi}_{2.4}\text{Sr}_{2.6}\text{Fe}_2\text{O}_{9+\delta}$ previously investigated [Y. Lepage, W. R. McKinnon, J. M. Tarascon, and P. Barboux, *Phys. Rev. B* **40**, 6810 (1989); O. Pérez, H. Leligny, D. Grebille, J. M. Grenèche, Ph. Labbé, D. Groult, and B. Raveau, *Phys. Rev. B* **55**, 1236 (1997)]. The study was carried out on a single crystal, using synchrotron radiation ($\lambda = 0.326$ Å). The crystal is monoclinic with cell parameters $a = 16.491(9)$ Å, $b = 5.481(3)$ Å, $c = 30.086(16)$ Å, $\beta = 91.39(2)^\circ$. The real structure of symmetry $P2_1/n$ appears as a small perturbation of the ideal structure with higher symmetry $B2/m$. The undulating $(001)_m$ layers of the modulated (m) phase built from one kind of cation (Bi, Sr, or Fe) are replaced by mixed layers. The waving of these layers is less regular than in the modulated phase because interrupted layers are connected. One of the most interesting results relates to the interrupted Bi layers: the isolated blocks composed of two adjacent infinite $[010]$ ribbons, six Bi atoms wide, are similar to the ordered part (condensed zones) of the Bi-2212 modulated phase. The Bi disordered regions (diluted zones) are missing in the double-collapsed phase. An original octahedral coordination is implied for the Bi atoms located near the Fe atoms in the same undulated mixed layer. Disorder phenomena have been observed in a complementary HREM study and appear as localized faults modifying mainly the length of the Bi ribbons. [S0163-1829(97)01229-0]

I. INTRODUCTION

Oxides belonging to the Bi-Sr-Ca-Cu-O system are well known, both for their superconducting properties and their structural characteristics. Up to now, an adequate relation between the corresponding modulated structures and their physical properties has not been completely established, partly because of the lack of an accurate description of the atomic locations and occupancies, and partly because of the possible existence of defects correlated to the modulations.^{1,2}

Various phases in the Bi-Sr-Cu-O, Bi-(Ba,Sr)-Cu-O, and Bi-Sr-Fe-O systems are structurally very similar to phases in the Bi-Sr-Ca-Cu-O system. Indeed, commensurate or incommensurate modulations occur in these phases and they are very similar to those observed in the Bi-Sr-Ca-Cu-O system. A new family of phases, the so-called “collapsed” phases,^{3–8} exists in these systems. The electron diffraction patterns of modulated and collapsed phases show similar features where small bands of higher intensity reflections alternate with larger bands of weaker intensity reflections. A structural study of the collapsed compounds is, thus, of interest in understanding the details of the modulated phases. Moreover, HREM images of the collapsed structures have often been interpreted with reference to the modulated structures.

In a preliminary model, slices of crystal are isolated in the original modulated structure and sheared. According to the type of shearing mechanism (one shift or two orthogonal shifts) we refer to either collapsed or double-collapsed phases. This shear leads to mixed cationic layers or to broken

layers instead of infinite homogeneous layers. Moreover, the sets of main and satellite reflections can be distinguished in the electron diffraction pattern of the modulated compounds. In contrast, in the collapsed phases, it is no longer possible to define two groups of reflections, and the pattern can be indexed as a whole according to the three-dimensional periodicity.

Structural models were proposed as a result of HREM studies for the following compounds: the collapsed phase $\text{Bi}_{15}\text{Ba}_7\text{Sr}_7\text{Cu}_6\text{O}_{42.5}$ (Ref. 3) and the three double-collapsed phases $\text{Bi}_6\text{Ba}_4\text{Cu}_2\text{O}_{15}$,⁴ $\text{Bi}_{16}\text{Sr}_{28}\text{Cu}_{17}\text{O}_{69+\delta}$,⁵ and $\text{Bi}_{13}\text{Ba}_2\text{Sr}_{25}\text{Fe}_{13}\text{O}_{66}$ (Ref. 6) related to the 2201 Bi-Cu modulated phase, 2212 Bi-Cu, and 2201-0201 intergrowth $\text{Bi}_2\text{Sr}_4\text{Fe}_2\text{O}_{10}$ (Ref. 7) modulated phases. Combining neutron and x-ray powder diffraction data with HREM observations, a structural model was proposed for the $\text{Bi}_2\text{Sr}_2\text{CuO}_6$ collapsed phase.⁸

A single-crystal structural study was needed to improve the understanding of these phases, to clarify the structural similarities with the modulated phases, and to investigate the original features peculiar of the sheared zones.

II. EXPERIMENT

A. Synthesis

Single crystals were prepared starting from a mixture of $\text{Sr}(\text{NO}_3)_2$, Bi_2O_3 , and Fe_2O_3 . The powders were weighed in the molar ratio Bi:1.33 Sr:2 Fe:1 and crushed in an agate mortar. An alumina crucible containing 10 g of this mixture was heated in the same way as for the synthesis of the $\text{Bi}_{2.4}\text{Sr}_{2.6}\text{Fe}_2\text{O}_{9+\delta}$ compound.⁹

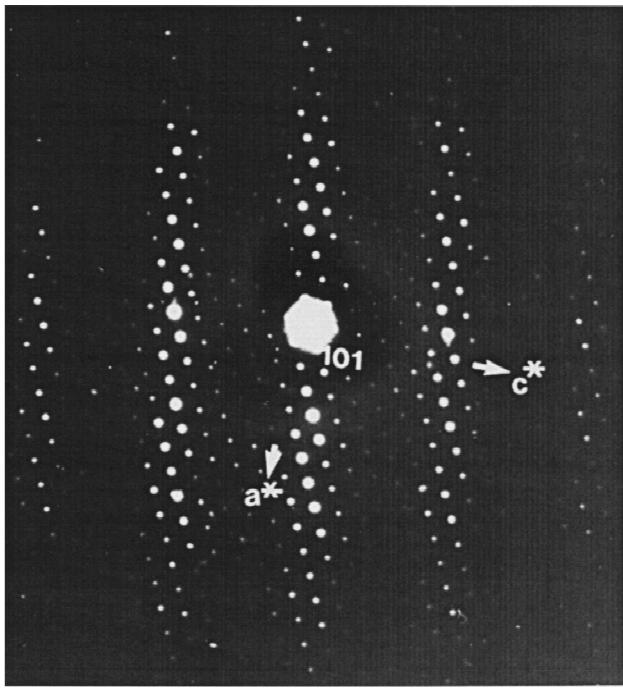


FIG. 1. Electron diffraction pattern of the $\text{Bi}_{6+x}\text{Sr}_{9-x}\text{Fe}_5\text{O}_{26}$ compound (zone axis $[010]$).

Single crystals grow as small dark needles along the $[010]$ direction with a diamond-shaped cross section. The quality of numerous crystals was tested using a Weissenberg camera. Two single monodomain crystals were selected for a complete diffraction study.

B. Symmetry

The different tested samples showed similar diffraction patterns: small bands of higher intensity reflections alternate with large bands of weaker intensities (Fig. 1). The electron diffraction patterns and the Weissenberg camera photographs are compatible with monoclinic symmetry. The unit cell parameters, $a = 16.491(9)$ Å, $b = 5.481(3)$ Å, $c = 30.086(16)$ Å, $\beta = 91.39(2)^\circ$, were refined by accurate centering of 25 independent reflections on an Enraf-Nonius CAD4 diffractometer. The crystals are also characterized by a distinct pseudo-translational symmetry. In fact two sets of reflections are observed: a set of very strong reflections with

$h+l=2n$, and a set of much weaker reflections with $h+l=2n+1$. This suggests a pseudo B -centered lattice, although the actual lattice is obviously primitive.

To reduce the correlations between the positional parameters¹⁰ during the refinement, a setting leading to a β value close to $\pi/2$ was chosen. This choice implies the non-standard $P2_1/n$ space group consistent with the reflection conditions $(0k0):k=2n$ and $(h0l):h+l=2n$. This space group appears as a subgroup of $B2/m$ which is interesting to consider in a starting model.

C. Data collection

The intensities of reflections of the first specimen were recorded at room temperature on an Enraf-Nonius CAD4 diffractometer using $\text{Mo } K_\alpha$ radiation. The number of weak reflections (hkl) with $h+l=2n+1$, which are the most sensitive to the atomic deviations from ideal positions described in the $B2/m$ space group, was insufficient to perform a satisfactory refinement of the structure in its primitive lattice.

This led us to collect data from a second crystal using the ID11 Material Sciences beamline of the European Synchrotron Radiation Facility.¹¹ A wavelength $\lambda = 0.326$ Å was chosen in order to reduce absorption effects. Data were recorded with a Thomson x-ray image intensifier coupled to a Princeton slow scan CCD camera. The detector was calibrated for spatial distortion using a Cu grid and for uniformity of sensitivity using an amorphous glass doped with Dy.¹² Data were collected in oscillations of 1° with 0.2° overlap. Images were corrected using FIT2D (Ref. 13) and integrated with DENZO.¹⁴ Data were subsequently scaled and merged. The registered pictures confirm the good diffraction quality of our sample (well-resolved spots without any observable diffuse streaks). The quality of the obtained data set was significantly improved, mainly for the reflections $h+l=2n+1$. The experimental details are summarized in Table I. The observed intensities were not corrected for absorption because it was found to be negligible: the linear absorption coefficient of the crystal at this wavelength is small ($\mu \approx 80 \text{ cm}^{-1}$). The size of the crystal section, $18 \times 18 \text{ } \mu\text{m}^2$, is also small and in spite of the length of the needle ($360 \text{ } \mu\text{m}$), the paths of the incident and diffracted beams do not vary significantly from one reflection to another.

TABLE I. Details of data collection.

Crystal size	$18 \times 18 \times 360 \text{ } \mu\text{m}^3$
Cell parameters ($T = 294 \text{ K}$)	$a = 16.491(9) \text{ Å}$, $b = 5.481(3) \text{ Å}$, $c = 30.086(16) \text{ Å}$, $\beta = 91.39(2)^\circ$
Space group	$P2_1/n$
Z , V	4, 2718 Å^3
Wavelength	0.326 Å
Index restrictions	$-26 \leq h \leq 26$, $0 \leq k \leq 8$, $0 \leq l \leq 46$
No. of reflections with $I \geq 3\sigma(I)$	2674
Absorption coefficient	80 cm^{-1}
No. of least squares parameters	246
Weighting scheme	$1/\sigma^2(F)$
Reliability factors (R/wR)	0.069/0.087

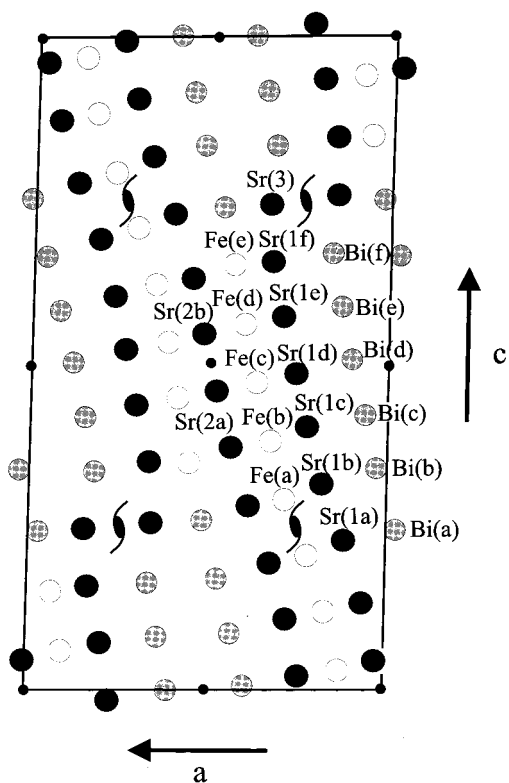


FIG. 2. Projection of the double collapsed $\text{Bi}_{6+x}\text{Sr}_{9-x}\text{Fe}_5\text{O}_{26}$ cationic structure along \vec{b} .

The electron diffraction study was carried out on a Jeol 200CX electron microscope. The HREM study was performed with a TOPCON 002B electron microscope operating at 200 kV and having a point resolution of 1.8 Å.

Electron probe microanalysis was performed with a Philips FEG-XL30 scanning electron microscope equipped with an EDS-LINK analysis system.

III. STRUCTURE REFINEMENTS

A preliminary model, assuming the space group $B2/m$, was found by direct methods using SIR92.¹⁵ High resolution microscopy suggests notable structural similarities between the present crystal and the modulated $\text{Bi}_{2.4}\text{Sr}_{2.6}\text{Fe}_2\text{O}_{9+\delta}$ phase which was previously studied.^{9,16,17} Atoms could be identified, therefore, by analogy with the already known structure using the interatomic distances. Only the cations were located in this first step. The atoms occupy special positions on the mirror planes ($y = \pm 1/4$) in the space group $B2/m$. The results were carefully verified by Patterson maps and then the x, z atomic coordinates of the cations were refined using the reflections with $h + l = 2n$ and SDS.¹⁸ The labeling of the cations is specified in Fig. 2 where the unit cell of the double-collapsed structure is represented.

In this first model it was not possible to locate all the oxygen atoms, from difference Fourier synthesis. Moreover, anomalously large thermal displacement parameters were observed along [010], especially for Bi atoms, inducing us to work within the real symmetry, that of the $P2_1/n$ space group. The mirror plane is lost in this group, and lowering of the translational symmetry from a face centered to a primi-

tive lattice is achieved as a result of atomic displacements along [010] from the ideal position, $y = \pm 1/4$. It should also be noted that two different structural hypotheses are possible and have to be tested within the $P2_1/n$ subgroup. Two adjacent Bi ribbons are symmetrically related either by a two-fold screw axis or by a center of inversion (Fig. 2). Considering only the primitive reflections, and assuming isotropic thermal motion, the Bi atoms were shifted 0.1 to 0.2 Å along [010] according to analysis of thermal displacement parameters obtained in space group $B2/m$. The hypothesis involving a center of inversion between adjacent bracketlike Bi ribbons led to a significantly better agreement. A new refinement of the x, y, z coordinates of the Bi atoms was then attempted, leading to a significant decrease of the R factor (from 0.42 to 0.15) for reflections with $h + l = 2n + 1$. This result clearly shows that the change of symmetry from $B2/m$ to $P2_1/n$ is mainly due to the small displacements of the Bi atoms from their ideal positions. All the oxygen atoms were located by alternating least squares refinement of the cation parameters and difference Fourier synthesis using the two groups of reflections, allowing a global refinement of the actual structure to be performed.

The thermal displacement parameters of the cations and oxygen atoms were treated as anisotropic and isotropic, respectively. Substitution of Bi for Sr on all the strontium sites adjacent to the Bi atoms was also considered, according to the results obtained for the modulated phase.^{9,17}

The structure refinement indicated some problems for Fe(e), Sr(3), Bi(a), and Bi(f). The Bi(a) and Bi(f) occupancies were found to be less than one which could be interpreted, as a substitution of Fe for Bi and/or Sr for Bi, respectively, consistent with their positions in the structure. A splitting and a spreading out of the electron density have also been observed on the Fourier difference maps at the Sr(3) site and Fe(e) site levels respectively (Figs. 3 and 4). The occupancy of the Fe site was found to be greater than one and a substitution of Bi for Fe was therefore considered. Two distinct sites, (a) and (b), were refined in the case of Sr(3). The (a) site which occurs in a row of Bi atoms was considered to be occupied by Bi, whereas the (b) site which is mainly occupied by Sr and only a small substitution of Bi for Sr, comparable with the similar occupation of the other Sr sites, was considered. This feature will be discussed further (Sec. IV C).

The atomic positions, thermal displacement parameters, and occupational parameters are summarized in Tables II and III. The oxygen atoms, labeled O(1) and O(2), are located within the interrupted iron layers; O(3) and O(4) are the apical oxygen atoms [O(4) is located across two broken iron layers]; O(5) is located in the bismuth layers. The letters used in the oxygen and cation notation have the same meaning and are related to the location of the atom along the \vec{c} direction.

IV. DISCUSSION

The present collapsed structure shows obvious similarities with the incommensurate 2212 iron phase.^{9,17} We recall the main structural properties of this modulated phase. The symmetry is orthorhombic with the unit cell parameters $a_m \approx 5.4$ Å, $b_m \approx 5.4$ Å, $c_m \approx 31.7$ Å and the superspace

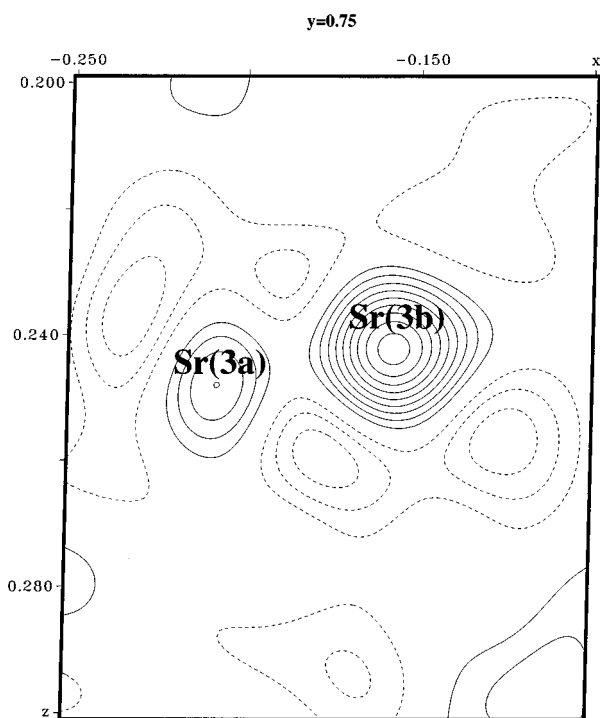


FIG. 3. Difference Fourier map ($y=0.75$) showing up the splitting of the Sr(3) atoms. Contours are drawn at intervals of $3 \bar{e} \text{ \AA}^{-3}$. Solid lines and short dashed lines represent positive and negative electron density, respectively.

group $Abmm(0,\beta,1)00s$. Owing to the modulation, the atoms are displaced off their average position to form undulated $(001)_m$ layers [Fig. 5(b)] which are composed of only one kind of cation (Bi, Sr, or Fe) and mixed cationic $(010)_m$ wavy planes. The $(001)_m$ layers will be labeled [BiO], [SrO], and [FeO₂], respectively. Running along \vec{c}_m , adjacent [BiO], [SrO], [FeO₂], [SrO], [FeO₂], [SrO], [BiO] layers form a slab. The modulation and curvature of each slab along \vec{c} is exactly out of phase with adjacent slabs [Fig. 5(b)]. For two adjacent [BiO] layers, this feature gives rise to shrinking and bulging zones, and within each [BiO] layer, diluted and condensed regions are formed.^{9,16,17} The shrinking zones (diluted regions) are characterized by a disorder resulting in a splitting of the Bi sites.

The main structural features of the so-called double-collapsed phase can be described with reference to the modulated structure [Fig. 5(b)]. Layers can still be distinguished, but they are now mixed cationic layers parallel to the $(70\bar{3})$ plane, with the following sequence: . . . 18Sr, 6Bi, 10Fe, 6Bi, 18Sr, The following approximate relationship between the basic cell translation directions of both structures can be established: $\vec{a}_m // \vec{b}$, $\vec{b}_m // (3\vec{a} + 7\vec{c})$, $\vec{c}_m // (10\vec{a} - \vec{c})$. It can also be shown that all these mixed layers are equivalent by translational symmetry; two adjacent mixed layers are related by the lattice translation $(\vec{a} + 2\vec{c})$.

It is important to have an accurate description of the different cation environments (Sec. IV A) in the collapsed phase in order to clarify what are the actual similarities and differences between both structures. Then it will be possible to propose a more general interpretation of the structure us-

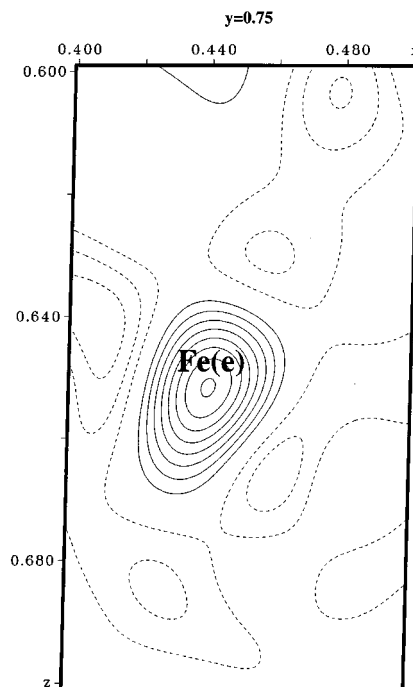


FIG. 4. Difference Fourier map ($y=0.75$) outlining the spreading of the electronic density, in the (\vec{a}, \vec{c}) plane, for the Fe(*e*) atoms. Contours are drawn at intervals of $3 \bar{e} \text{ \AA}^{-3}$. Solid lines and short dashed lines represent positive and negative electron densities, respectively.

ing 2212-type blocks and an original accommodation region (Sec. IV B). The ideal ordered model of this region is described. The deviation from this idealized structure, including the problems evidenced for Bi(*a*), Bi(*f*), Sr(3), and Fe(*e*) atoms, are the subject of Sec. IV C.

A. Cation environment

The Fe-O, Sr-O, and Bi-O distances are listed in Table IV.

All the Fe cations have “5 + 1” nearest neighbors so that their coordination can be described in terms of either FeO₅ pyramids or as strongly distorted FeO₆ octahedra. The apical distance Fe-O (2.4–2.6 Å) inside these octahedra, is indeed much larger than all the other Fe-O distances (<2 Å). Fe octahedra form ribbons parallel to $(001)_m$ which are ten octahedra wide along \vec{b}_m (Fig. 6). Within each ribbon, three kinds of octahedra can be distinguished: the first (labeled *b*, *c* and *d* in Fig. 6) is connected to four other octahedra in the same ribbon and to a fifth apical octahedron in the adjacent ribbon; the second (*e*) provides the connection with the Bi ribbon and is only connected to two FeO₆ octahedra in the same ribbon. Together, these two kinds (*b*, *c*, *d*, and *e*) form double pyramidal Fe ribbons (thick lines in Fig. 6) which are very similar to those observed near the Bi condensed regions of the 2212 modulated structure. The third kind (*a*), in the middle of the ribbon, is only connected to Fe octahedra in the same ribbon; it is located between two Bi ribbons.

One can see a reversal of their apical Fe-O bonds with respect to each other (thick lines in Fig. 6) related to the location of the 2₁ screw axis between them.

TABLE II. Crystallographic parameters.

Atom	x	y	z	u_{11}	u_{22}	u_{33}	u_{12}	u_{13}	u_{23}
Bi(<i>a</i>)	-0.0245(1)	0.25 ^a	0.2449(1)	0.0075(5)	0.0087(10)	0.116(7)	0.00 ^a	0.0024(5)	0.00 ^a
Bi(<i>b</i>)	0.0232(1)	0.7355(5)	0.3350(1)	0.0091(5)	0.0082(10)	0.0094(7)	-0.0009(7)	0.0018(4)	-0.0003(9)
Bi(<i>c</i>)	0.0636(1)	0.2672(6)	0.4163(1)	0.0069(5)	0.0113(11)	0.0124(7)	0.00 ^a	0.0011(4)	0.0010(11)
Bi(<i>d</i>)	0.1030(1)	0.7216(5)	0.4998(1)	0.0077(5)	0.0092(10)	0.0105(7)	0.0008(7)	0.0018(4)	0.0012(9)
Bi(<i>e</i>)	0.1367(1)	0.2784(5)	0.5828(1)	0.0085(5)	0.0128(12)	0.0125(8)	0.0006(7)	0.0040(5)	0.0007(10)
Bi(<i>f</i>)	0.1658(1)	0.7361(6)	0.6689(1)	0.0092(6)	0.0143(11)	0.0097(8)	0.00 ^a	0.0033(5)	0.00 ^a
Sr(2 <i>a</i>)	0.4419(2)	0.75 ^a	0.3665(2)	0.0167(14)	0.005(2)	0.0103(16)	0.00 ^a	0.00 ^a	0.00 ^a
Sr(2 <i>b</i>)	0.4821(2)	0.2465(7)	0.4554(2)	0.0109(11)	0.0071(18)	0.0077(13)	0.00 ^a	-0.0016(9)	0.00 ^a
Sr(1 <i>a</i>)	0.3856(2)	0.2462(10)	0.2767(2)	0.0256(16)	0.012(2)	0.0094(17)	-0.0037(18)	0.0044(13)	0.00 ^a
Sr(1 <i>b</i>)	0.1762(2)	0.25 ^a	0.3109(2)	0.0205(14)	0.007(2)	0.0085(15)	0.00 ^a	-0.0014(11)	0.00 ^a
Sr(1 <i>c</i>)	0.2232(2)	0.7565(9)	0.3959(1)	0.0153(11)	0.007(2)	0.0078(14)	0.0023(15)	-0.0051(1)	0.0026(17)
Sr(1 <i>d</i>)	0.2623(2)	0.25 ^a	0.4814(1)	0.0143(11)	0.009(2)	0.0084(14)	0.00 ^a	0.00 ^a	0.00 ^a
Sr(1 <i>e</i>)	0.2979(2)	0.7581(12)	0.5689(1)	0.0177(12)	0.0052(19)	0.0088(14)	0.00 ^a	-0.0018(10)	-0.005(4)
Sr(1 <i>f</i>)	0.3297(13)	0.2533(13)	0.6551(2)	0.038(2)	0.008(2)	0.0097(15)	0.00 ^a	-0.0038(12)	0.00 ^a
Sr(3 <i>a</i>)	-0.2091(8)	0.728(4)	0.2445(6)	0.03(1)	0.02(1)	0.04(1)	0.008(7)	0.00 ^a	0.014(10)
Sr(3 <i>b</i>)	-0.1596(3)	0.7393(11)	0.2442(2)	0.024(2)	0.007(3)	0.012(2)	0.00 ^a	0.0026(14)	0.00 ^a
Fe(<i>a</i>)	0.2826(3)	0.75 ^a	0.2933(2)	0.023(3)	0.0100(4)	0.005(3)	0.00 ^a	-0.004(2)	0.00 ^a
Fe(<i>b</i>)	0.3329(3)	0.2533(15)	0.3802(2)	0.008(2)	0.006(3)	0.009(3)	0.003(2)	0.00 ^a	0.004(3)
Fe(<i>c</i>)	0.3708(3)	0.75 ^a	0.4688(2)	0.007(2)	0.011(4)	0.007(3)	0.00 ^a	0.00 ^a	0.00 ^a
Fe(<i>d</i>)	0.4066(3)	0.25 ^a	0.5576(2)	0.007(2)	0.010(3)	0.009(3)	0.00 ^a	0.00 ^a	0.00 ^a
Fe(<i>e</i>)	0.4405(3)	0.75 ^a	0.6501(2)	0.018(2)	0.014(3)	0.035(3)	0.00 ^a	-0.005(2)	0.00 ^a
Atom	x	y	z	U_{iso}					
O(1 <i>a</i>)	0.248(3)	0.50 ^a	0.2500(16)	0.015(5)					
O(1 <i>b</i>)	0.301(2)	0.00 ^a	0.3377(6)	0.011(6)					
O(2 <i>b</i>)	0.294(2)	0.50 ^a	0.3376(6)	0.006(2)					
O(1 <i>c</i>)	0.343(2)	0.00 ^a	0.4242(11)	0.004(2)					
O(2 <i>c</i>)	0.341(3)	0.50 ^a	0.4283(16)	0.016(8)					
O(1 <i>d</i>)	0.381(3)	0.00 ^a	0.5167(13)	0.011(5)					
O(2 <i>d</i>)	0.375(3)	0.50 ^a	0.5126(13)	0.007(4)					
O(1 <i>e</i>)	0.414(3)	0.00 ^a	0.5998(17)	0.029(10)					
O(2 <i>e</i>)	0.411(3)	0.50 ^a	0.6064(13)	0.011(4)					
O(1 <i>f</i>)	0.4459(16)	0.00 ^a	0.6918(12)	0.008(4)					
O(2 <i>f</i>)	0.430(3)	0.50 ^a	0.6932(19)	0.027(12)					
O(3 <i>a</i>)	0.1400(16)	0.75 ^a	0.3163(11)	0.018(7)					
O(3 <i>b</i>)	0.1820(14)	0.204(7)	0.4025(10)	0.007(3)					
O(3 <i>c</i>)	0.2241(14)	0.771(9)	0.4864(10)	0.008(4)					
O(3 <i>d</i>)	0.2609(14)	0.240(11)	0.5735(10)	0.013(5)					
O(3 <i>e</i>)	0.2873(15)	0.784(9)	0.6625(11)	0.017(7)					
O(3 <i>f</i>)	0.3148(17)	0.229(10)	0.7572(12)	0.014(4)					
O(4 <i>a</i>)	0.3987(14)	0.75 ^a	0.2741(10)	0.013(3)					
O(4 <i>b</i>)	0.4442(11)	0.25 ^a	0.3635(14)	0.016(5)					
O(4 <i>c</i>)	0.4819(14)	0.731(6)	0.4539(11)	0.014(5)					
O(5 <i>a</i>)	-0.011(2)	0.666(8)	0.2701(14)	0.029(12)					
O(5 <i>b</i>)	0.0375(16)	0.356(7)	0.3486(1)	0.012(5)					
O(5 <i>c</i>)	0.078(2)	0.644(7)	0.4285(13)	0.018(8)					
O(5 <i>d</i>)	0.1118(17)	0.349(7)	0.5043(12)	0.016(6)					
O(5 <i>e</i>)	0.1415(16)	0.664(7)	0.5788(11)	0.013(5)					
O(5 <i>f</i>)	0.1677(16)	0.339(7)	0.6621(12)	0.014(5)					

^aWere fixed during the refinement because their variation from the present values were insignificant.

TABLE III. Occupancy probabilities of different cationic sites.

	%Bi	%Sr	%Fe
Bi(<i>a</i>)	88.88(1)	-	11.12(1)
Bi(<i>f</i>)	82.73(1)	17.27(1)	-
Sr(1 <i>a</i>)	-	100 ^a	-
Sr(1 <i>b</i>)	4.14(1)	95.86(1)	-
Sr(1 <i>c</i>)	6.81(1)	93.19(1)	-
Sr(1 <i>d</i>)	8.26(1)	91.74(1)	-
Sr(1 <i>e</i>)	10.70(1)	89.30(1)	-
Sr(1 <i>f</i>)	12.31(2)	87.69(2)	-
Sr(3 <i>a</i>)	14.03(1)	-	-
Sr(3 <i>b</i>)	4.82(1)	81.18(1)	-
Fe(<i>e</i>)	16.44(2)	-	83.56(2)

^aWere fixed during the refinement because their variation from the present values were insignificant.

Three different coordinations are observed for the Sr atoms. The first two were already seen in the incommensurate phase: Sr(1) has the ninefold environment typical of the rock-salt-type structure between one $[\text{FeO}_2]$ layer and one $[\text{BiO}]$ layer and Sr(2) has the 12-fold coordination characteristic of the perovskite-type structure between the $[\text{FeO}_2]$ layers. Sr(3) presents an original eightfold coordination, which results from the particular location of this cation in the continuation of a row of Bi atoms.

The stacking of two adjacent mixed layers results in the periodic arrangement of pairs of infinite Bi ribbons parallel to the $(001)_m$ plane [Fig. 5(a)]. These double ribbons are six atoms wide. Their bracketlike configuration is particularly visible in the HREM images (Fig. 2a in Ref. 19). The position of these double Bi ribbons is characterized by a relative shift of ~ 2.1 Å. Hence, the Bi and O atoms of two adjacent

ribbons are not stacked exactly on top of each other, as was the case in the modulated structure. This shift results in a discontinuity of the mixed cationic $(010)_m$ planes which are continuous in the modulated structure. Nevertheless, the Bi ribbon of the collapsed phase presents exactly the same configuration of double BiO chains running along \vec{b}_m as the equivalent part of the $[\text{BiO}]$ layer of the modulated phase [Fig. 5(b)].

The similarity between the collapsed and the modulated phase is further confirmed by the similarity of the Bi-O distances and the O-Bi-O angles (Table IV). Three of the bismuth cations, Bi(*b*), Bi(*c*), and Bi(*f*), are characterized by two short in-plane Bi-O distances, ranging from 2.05 to 2.24 Å (dark lines in Fig. 7), and one short out-of plane Bi-O distance (perpendicular to the $[\text{BiO}]$ ribbon), ranging from 2.03 to 2.08 Å. Thus, the corresponding coordination can be described as a BiO_3L tetrahedron, considering that the electronic lone pair of Bi(III) is directed perpendicularly to the “ O_3 ” plane, as schematically shown in Fig. 7. In this case, the behavior of Bi(*b*), Bi(*c*), and Bi(*f*) is very similar to that observed for Bi in the “2212” modulated structure where BiO_3L tetrahedral coordination was also observed. Nevertheless, it is worth pointing out that each of these atoms has an additional O atom located at 2.76–2.97 Å (gray lines in Fig. 7) so that the coordination of these three Bi cations can be considered as intermediate between the tetrahedral BiO_3L and distorted pyramidal BiO_4L . The two cations, Bi(*d*) and Bi(*e*), have three short in-plane Bi-O distances, ranging from 2.05 to 2.46 Å (black lines in Fig. 7) and one short out-of plane Bi-O distance ranging from 2.06 to 2.08 Å, so that their lone pair is approximately directed along \vec{b} (Fig. 7). Consequently, the coordination of these two atoms can be described as BiO_4L pyramids. The relative shift between two adjacent Bi ribbons results in a very unusual configuration for Bi(*a*): it is close to that of Fe(*e*) atom in the same mixed layer and is inserted between two $[\text{SrO}]$ interrupted layers. This Bi atom occupies an “Fe-type” position: it forms a junction with the adjacent $[\text{FeO}_2]$ interrupted layer by two short bonds with O(1*f*) and O(2*f*) atoms of square planar iron (2.16–2.19 Å). An intermediate Bi(*a*)-O distance of 2.4 Å is achieved with the O(5) atom belonging to the Bi(*b*) tetrahedron. Thus, for this atom, one observes three short in-plane Bi-O distances with a “ BiO_3 ” configuration similar to that observed for other Bi in the chain. However, Bi(*a*) differs from the other bismuth atoms because of the existence of two apical Bi-O bonds, with the result that it is surrounded by five O atoms. This coordination can be described as distorted octahedral BiO_5L , with the lone pair forming the fourth vertex of the basal plane of this octahedron as shown in Fig. 7.

B. Comparison between the collapsed and modulated phases

As has already been mentioned, the collapsed and the modulated phases show great similarities concerning the cation coordinations and the existence of specific cationic stacking or layers.

According to the previous HREM study, the collapsed phase has been interpreted as a regular stacking of two kinds of slices parallel to (001) : only one slice (*D*-2212 in Fig. 6) is characterized by the cationic sequence of the 2212 modu-

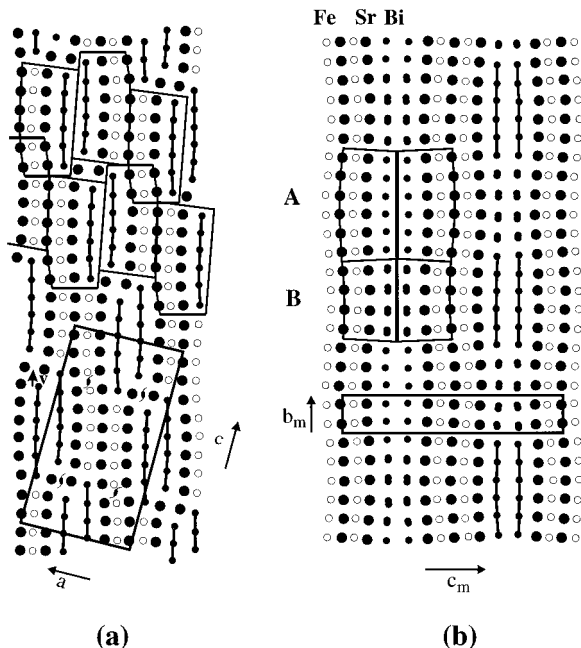


FIG. 5. Structural comparison between the double-collapsed phase (a) (projection along \vec{b}_m) and the modulated phase (b) (projection along \vec{a}_m). Only cations are shown.

TABLE IV. Cation-oxygen distances (Å) and O-Bi-O angles ($^{\circ}$). Symmetry codes: I: x, y, z ; II: $x - 1/2, 1/2 - y, z - 1/2$; III: $1/2 - x, y - 1/2, 1/2 - z$; IV: $x, y - 1, z$; V: $x, 1 + Y, z$; VI: $-x, 1 - y, 1 - z$; VII: $1/2 - x, 1/2 + y, 3/2 - z$; VIII: $1 - x, -y, 1 - z$; IX: $1 - x, 1 - y, 1 - z$; X: $1/2 - x, 3/2 - y, z - 1/2$; XI: $1/2 - x, 1/2 + y, 1/2 - z$.

Bi(<i>a</i>)-O(1 <i>f</i>) ^{II}	2.16(3)	O(1 <i>f</i>) ^{II} -Bi(<i>a</i>)-O(2 <i>f</i>) ^{II}	78(2)		
Bi(<i>a</i>)-O(2 <i>f</i>) ^{II}	2.19(5)	O(1 <i>f</i>) ^{II} -Bi(<i>a</i>)-O(3 <i>g</i>) ^{II}	83(2)		
Bi(<i>a</i>)-O(3 <i>a</i>) ^{III}	2.16(3)	O(1 <i>f</i>) ^{II} -Bi(<i>a</i>)-O(3 <i>a</i>) ^{III}	90(1)		
Bi(<i>a</i>)-O(5 <i>a</i>) ^I	2.41(5)	O(1 <i>f</i>) ^{II} -Bi(<i>a</i>)-O(5 <i>a</i>) ^{II}	70(2)		
Bi(<i>a</i>)-O(3 <i>g</i>) ^{II}	2.68(3)	O(2 <i>f</i>) ^{II} -Bi(<i>a</i>)-O(3 <i>g</i>) ^{II}	79(2)		
Bi(<i>a</i>)-O(5 <i>a</i>) ^{IV}	3.29(5)	O(2 <i>f</i>) ^{II} -Bi(<i>a</i>)-O(3 <i>a</i>) ^{III}	97(2)		
Bi(<i>a</i>)-O(5 <i>b</i>) ^I	3.31(4)	O(3 <i>g</i>) ^{II} -Bi(<i>a</i>)-O(5 <i>a</i>) ^I	90(2)		
		O(3 <i>a</i>) ^{III} -Bi(<i>a</i>)-O(5 <i>a</i>) ^I	90(1)		
Bi(<i>b</i>)-O(3 <i>b</i>) ^I	2.08(3)	O(3 <i>b</i>) ^I -Bi(<i>b</i>)-O(5 <i>a</i>) ^I	90(2)		
Bi(<i>b</i>)-O(5 <i>a</i>) ^I	2.05(4)	O(3 <i>b</i>) ^I -Bi(<i>b</i>)-O(5 <i>b</i>) ^I	89(1)		
Bi(<i>b</i>)-O(5 <i>b</i>) ^I	2.13(4)	O(5 <i>a</i>) ^I -Bi(<i>b</i>)-O(5 <i>b</i>) ^I	92(2)		
Bi(<i>b</i>)-O(5 <i>b</i>) ^V	3.43(4)	O(5 <i>b</i>) ^I -Bi(<i>b</i>)-O(5 <i>c</i>) ^I	68(2)		
Bi(<i>b</i>)-O(5 <i>c</i>) ^I	2.97(4)	O(5 <i>b</i>) ^I -Bi(<i>b</i>)-O(5 <i>f</i>) ^{VI}	89(2)		
Bi(<i>b</i>)-O(5 <i>f</i>) ^{VI}	3.18(3)				
Bi(<i>c</i>)-O(3 <i>c</i>) ^I	2.03(3)	O(3 <i>c</i>) ^I -Bi(<i>c</i>)-O(5 <i>b</i>) ^I	91(1)		
Bi(<i>c</i>)-O(5 <i>b</i>) ^I	2.13(4)	O(3 <i>c</i>) ^I -Bi(<i>c</i>)-O(5 <i>c</i>) ^I	96(2)		
Bi(<i>c</i>)-O(5 <i>c</i>) ^I	2.11(4)	O(5 <i>b</i>) ^I -Bi(<i>c</i>)-O(5 <i>c</i>) ^I	88(2)		
Bi(<i>c</i>)-O(5 <i>d</i>) ^I	2.78(4)	O(5 <i>c</i>) ^I -Bi(<i>c</i>)-O(5 <i>d</i>) ^I	69(2)		
Bi(<i>c</i>)-O(5 <i>c</i>) ^V	3.44(4)	O(5 <i>d</i>) ^I -Bi(<i>c</i>)-O(5 <i>e</i>) ^I	102(2)		
Bi(<i>c</i>)-O(5 <i>e</i>) ^{VI}	3.41(3)				
Bi(<i>d</i>)-O(3 <i>d</i>) ^I	2.06(3)	O(3 <i>d</i>) ^I -Bi(<i>d</i>)-O(5 <i>c</i>) ^I	90(2)		
Bi(<i>d</i>)-O(5 <i>c</i>) ^I	2.22(4)	O(3 <i>d</i>) ^I -Bi(<i>d</i>)-O(5 <i>d</i>) ^I	94(2)		
Bi(<i>d</i>)-O(5 <i>d</i>) ^I	2.05(4)	O(3 <i>d</i>) ^I -Bi(<i>d</i>)-O(5 <i>e</i>) ^I	89(1)		
Bi(<i>d</i>)-O(5 <i>e</i>) ^I	2.46(4)	O(5 <i>c</i>) ^I -Bi(<i>d</i>)-O(5 <i>d</i>) ^I	83(2)		
Bi(<i>d</i>)-O(5 <i>d</i>) ^V	3.45(4)	O(5 <i>d</i>) ^I -Bi(<i>d</i>)-O(5 <i>e</i>) ^I	78(2)		
Bi(<i>d</i>)-O(5 <i>d</i>) ^{VI}	3.56(3)				
Bi(<i>e</i>)-O(3 <i>e</i>) ^I	2.08(3)	O(3 <i>e</i>) ^I -Bi(<i>e</i>)-O(5 <i>d</i>) ^I	92(1)		
Bi(<i>e</i>)-O(5 <i>e</i>) ^I	2.12(4)	O(3 <i>e</i>) ^I -Bi(<i>e</i>)-O(5 <i>e</i>) ^I	93(2)		
Bi(<i>e</i>)-O(5 <i>d</i>) ^I	2.42(4)	O(3 <i>e</i>) ^I -Bi(<i>e</i>)-O(5 <i>f</i>) ^I	88(1)		
Bi(<i>e</i>)-O(5 <i>f</i>) ^I	2.45(4)	O(5 <i>d</i>) ^I -Bi(<i>e</i>)-O(5 <i>e</i>) ^I	78(2)		
Bi(<i>e</i>)-O(5 <i>e</i>) ^{IV}	3.37(4)	O(5 <i>e</i>) ^I -Bi(<i>e</i>)-O(5 <i>f</i>) ^I	85(2)		
Bi(<i>e</i>)-O(5 <i>c</i>) ^{VI}	3.57(3)				
Bi(<i>f</i>)-O(3 <i>f</i>) ^I	2.03(3)	O(3 <i>f</i>) ^I -Bi(<i>f</i>)-O(3 <i>g</i>) ^{VII}	89(2)		
Bi(<i>f</i>)-O(3 <i>g</i>) ^{VII}	2.24(4)	O(3 <i>f</i>) ^I -Bi(<i>f</i>)-O(5 <i>e</i>) ^I	93(2)		
Bi(<i>f</i>)-O(5 <i>f</i>) ^I	2.19(4)	O(3 <i>f</i>) ^I -Bi(<i>f</i>)-O(5 <i>f</i>) ^I	96(2)		
Bi(<i>f</i>)-O(5 <i>e</i>) ^I	2.76(4)	O(5 <i>e</i>) ^I -Bi(<i>f</i>)-O(5 <i>f</i>) ^I	77(2)		
Bi(<i>f</i>)-O(5 <i>f</i>) ^V	3.31(4)	O(3 <i>g</i>) ^{VII} -Bi(<i>f</i>)-O(5 <i>f</i>) ^I	94(2)		
Bi(<i>f</i>)-O(5 <i>f</i>) ^{VI}	3.42(3)				
Sr(2 <i>a</i>)-O(1 <i>b</i>) ^V	2.81(4)	Sr(2 <i>b</i>)-O(1 <i>c</i>) ^I	2.80(3)	Sr(1 <i>a</i>)-O(2 <i>a</i>) ^I	2.77(4)
Sr(2 <i>a</i>)-O(2 <i>b</i>) ^I	2.90(3)	Sr(2 <i>b</i>)-O(2 <i>c</i>) ^I	2.82(4)	Sr(1 <i>a</i>)-O(2 <i>a</i>) ^{III}	2.68(4)
Sr(2 <i>a</i>)-O(1 <i>c</i>) ^V	2.77(3)	Sr(2 <i>b</i>)-O(1 <i>d</i>) ^I	2.85(4)	Sr(1 <i>a</i>)-O(1 <i>b</i>) ^I	2.69(3)
Sr(2 <i>a</i>)-O(2 <i>c</i>) ^I	2.87(5)	Sr(2 <i>b</i>)-O(1 <i>d</i>) ^{VIII}	2.74(4)	Sr(1 <i>a</i>)-O(2 <i>b</i>) ^I	2.77(3)
Sr(2 <i>a</i>)-O(1 <i>e</i>) ^{IX}	2.90(4)	Sr(2 <i>b</i>)-O(2 <i>d</i>) ^I	2.86(4)	Sr(1 <i>a</i>)-O(5 <i>a</i>) ^{III}	2.57(4)
Sr(2 <i>a</i>)-O(2 <i>e</i>) ^{IX}	2.88(3)	Sr(2 <i>b</i>)-O(2 <i>d</i>) ^{IX}	2.88(4)	Sr(1 <i>a</i>)-O(4 <i>a</i>) ^I	2.76(3)
Sr(2 <i>a</i>)-O(1 <i>f</i>) ^{IX}	2.91(3)	Sr(2 <i>b</i>)-O(1 <i>e</i>) ^{VIII}	2.77(4)	Sr(1 <i>a</i>)-O(3 <i>b</i>) ^{III}	2.83(4)
Sr(2 <i>a</i>)-O(2 <i>f</i>) ^{IX}	3.12(5)	Sr(2 <i>b</i>)-O(2 <i>e</i>) ^{IX}	2.93(4)	Sr(1 <i>a</i>)-O(3 <i>a</i>) ^{IV}	2.729(6)
Sr(2 <i>a</i>)-O(3 <i>a</i>) ^I	2.85(3)	Sr(2 <i>b</i>)-O(4 <i>a</i>) ^I	2.82(4)	Sr(1 <i>a</i>)-O(3 <i>a</i>) ^I	2.770(6)
Sr(2 <i>a</i>)-O(4 <i>a</i>) ^I	2.74(1)	Sr(2 <i>b</i>)-O(4 <i>b</i>) ^{IV}	2.82(4)		

TABLE IV. (Continued).

Sr(2a)-O(4a) ^V	2.74(1)	Sr(2b)-O(4b) ^I	2.66(4)		
Sr(2a)-O(4b) ^I	2.70(4)	Sr(2b)-O(4b) ^{IX}	2.78(4)		
Sr(1b)-O(2a) ^I	2.59(5)	Sr(1c)-O(1b) ^V	2.57(3)	Sr(1d)-O(1c) ^I	2.59(3)
Sr(1b)-O(2a) ^{III}	2.63(5)	Sr(1c)-O(2b) ^I	2.55(2)	Sr(1d)-O(2c) ^I	2.49(4)
Sr(1b)-O(1b) ^I	2.58(3)	Sr(1c)-O(1c) ^V	2.52(3)	Sr(1d)-O(1d) ^I	2.60(4)
Sr(1b)-O(2b) ^I	2.50(3)	Sr(1c)-O(2c) ^I	2.56(4)	Sr(1d)-O(2d) ^I	2.47(3)
Sr(1b)-O(3b) ^{IV}	2.797(5)	Sr(1c)-O(3b) ^I	2.70(3)	Sr(1d)-O(3c) ^I	2.70(3)
Sr(1b)-O(3b) ^I	2.797(5)	Sr(1c)-O(3c) ^I	3.11(4)	Sr(1d)-O(3d) ^{IV}	2.71(5)
Sr(1b)-O(3c) ^I	2.77(3)	Sr(1c)-O(3c) ^V	2.55(4)	Sr(1d)-O(3d) ^I	2.93(5)
Sr(1b)-O(3a) ^{III}	2.81(3)	Sr(1c)-O(3d) ^I	2.72(3)	Sr(1d)-O(3e) ^I	2.77(3)
Sr(1b)-O(5b) ^I	2.64(3)	Sr(1c)-O(5c) ^I	2.68(4)	Sr(1d)-O(5d) ^I	2.65(3)
Sr(1e)-O(1d) ^V	2.49(4)	Sr(1f)-O(1e) ^I	2.59(4)	Sr(3b)-O(1f) ^{II}	2.71(4)
Sr(1e)-O(2d) ^I	2.57(4)	Sr(1f)-O(2e) ^I	2.43(4)	Sr(3b)-O(2f) ^X	2.59(5)
Sr(1e)-O(1e) ^V	2.49(4)	Sr(1f)-O(1f) ^I	2.59(3)	Sr(3b)-O(3f) ^X	2.59(4)
Sr(1e)-O(2e) ^I	2.58(3)	Sr(1f)-O(2f) ^I	2.41(5)	Sr(3b)-O(3g) ^{VI}	2.56(3)
Sr(1e)-O(3d) ^I	2.74(3)	Sr(1f)-O(3e) ^I	2.68(3)	Sr(3b)-O(3g) ^{II}	2.63(6)
Sr(1e)-O(3e) ^I	2.91(6)	Sr(1f)-O(3f) ^{IV}	2.67(5)	Sr(3b)-O(3g) ^X	2.97(6)
Sr(1e)-O(3e) ^V	2.71(6)	Sr(1f)-O(3f) ^I	3.00(5)	Sr(3b)-O(5a) ^I	2.58(4)
Sr(1e)-O(3f) ^I	2.83(4)	Sr(1f)-O(3g) ^I	3.09(4)	Sr(3b)-O(5f) ^{VI}	2.86(4)
Sr(1e)-O(5e) ^I	2.65(3)	Sr(1f)-O(5f) ^I	2.72(3)		
Fe(a)-O(2a) ^I	1.97(4)	Fe(b)-O(1b) ^I	1.95(2)	Fe(c)-O(1c) ^V	1.96(3)
Fe(a)-O(2a) ^{XI}	1.95(4)	Fe(b)-O(2b) ^I	1.95(2)	Fe(c)-O(2c) ^I	1.89(3)
Fe(a)-O(1b) ^V	1.93(2)	Fe(b)-O(1c) ^I	1.92(3)	Fe(c)-O(1d) ^V	1.99(3)
Fe(a)-O(2b) ^I	1.92(2)	Fe(b)-O(2c) ^I	1.98(4)	Fe(c)-O(2d) ^I	1.90(3)
Fe(a)-O(3b) ^I	2.40(3)	Fe(b)-O(3c) ^I	2.61(3)	Fe(c)-O(3d) ^I	2.49(3)
Fe(a)-O(3a) ^I	2.01(3)	Fe(b)-O(4a) ^I	1.91(3)	Fe(c)-O(4b) ^I	1.90(3)
Fe(d)-O(1d) ^I	1.88(3)	Fe(e)-O(1e) ^V	2.08(4)		
Fe(d)-O(2d) ^I	1.99(3)	Fe(e)-O(2e) ^I	1.96(3)		
Fe(d)-O(1e) ^I	1.87(4)	Fe(e)-O(1f) ^V	1.85(3)		
Fe(d)-O(2e) ^I	2.00(4)	Fe(e)-O(2f) ^I	1.90(4)		
Fe(d)-O(3e) ^I	2.46(3)	Fe(e)-O(3f) ^I	2.57(3)		
Fe(d)-O(4b) ^{IX}	1.88(3)	Fe(e)-O(4a) ^{IX}	1.95(3)		

lated phase. Our present results agree with this interpretation, regardless of the previously mentioned shift between Bi ribbons. Moreover, two successive *D*-2212 slices are related to each other by a 2_1 screw axis, and not by a simple translation. The resulting structure cannot, therefore, be described as a pure sheared structure. The second kind of slice (*E* in Fig. 6), which corresponds to the two adjacent Fe(*a*)O₆ octahedra of the Fe ribbons, was interpreted as a zone allowing the accommodation of the proposed shearing mechanism. All the original Fe(*a*), Sr(3), and Bi(*a*) environments are localized in this slice.

More accurately, the relative cationic positions are exactly the same in infinite atomic blocks along the \vec{b} or along the \vec{a}_m directions of both structures. These blocks, labeled *A*, are drawn in Fig. 5. They consist of a stacking of ribbons of 6 Bi, 6 Sr, 6 Fe, and 6 Sr atoms and correspond to a half slab of the modulated phase between the two disordered diluted regions, labeled *B*.

The difference between the two structures is in how these elementary blocks are connected. In the modulated phase, the blocks *A* and *B* are directly stacked on top of each other in the same direction, \vec{c}_m , forming the cationic (010)_{*m*}

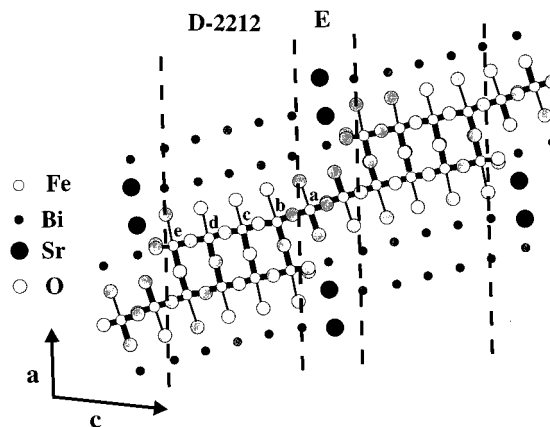


FIG. 6. Scheme of the Fe-O bonds in the double-collapsed phase. The thick and thin dark segments symbolize the shorter and the longer Fe-O distances, respectively. The dashed lines outline the *D*-2212 and *E* slices (see text).

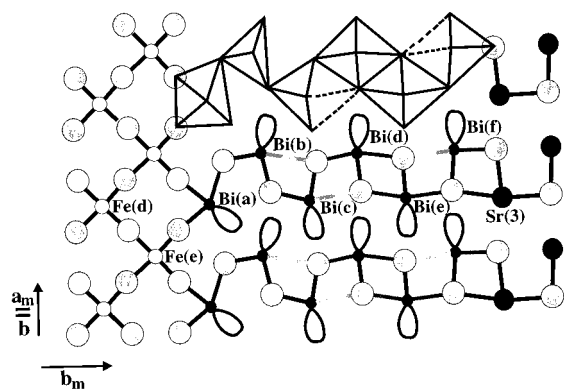


FIG. 7. Connection between the FeO_2 , BiO , and SrO ribbons within a same mixed layer. Both the bonding scheme and the arrangement of the Bi polyhedra including the electron lone pairs are shown. The dark, dark grey, and pale grey segments symbolize the strong, intermediate, and weak bonds respectively.

planes. On the contrary, two adjacent blocks are shifted with respect to each other by a translation \vec{v} [Fig. 5(a)] in the double-collapsed one.

The blocks labeled *B* [Fig. 5(b)], present in the modulated phase, are missing in the collapsed phase: these blocks are characterized both by a static disorder phenomenon which was observed in the modulated $[\text{BiO}]$ layers² and by an almost regular octahedral environment of the Fe atom, with apical Fe-O distances shorter than 2.2 Å. We can now see that in the collapsed phase there is no any disorder phenomena in the double Bi ribbon or any apical Fe-O distance shorter than 2.4 Å.

Other differences can also be noted. First, there are now common atoms, corresponding to the two middle $\text{Fe}(a)\text{O}_6$ octahedra of the $[\text{FeO}_2]$ ribbons, between the *A* blocks. Second, two supplementary Sr atoms [Sr(3)] are located between the four *A* blocks and have no equivalent in the modulated phase. They are characterized by an original eightfold coordination which is likely to play a part in the bonding scheme of this zone (Fig. 8). Third, the Bi(*a*) atom also has a very

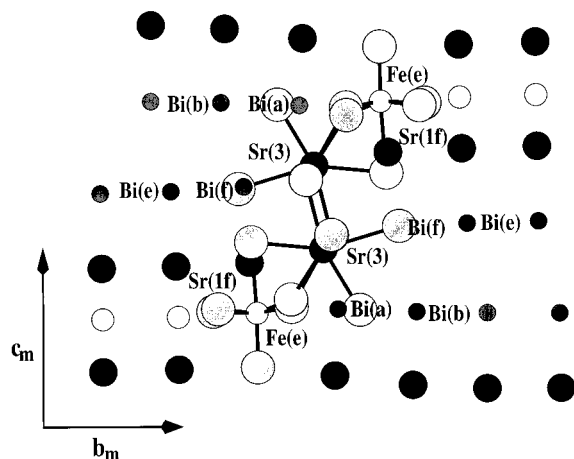
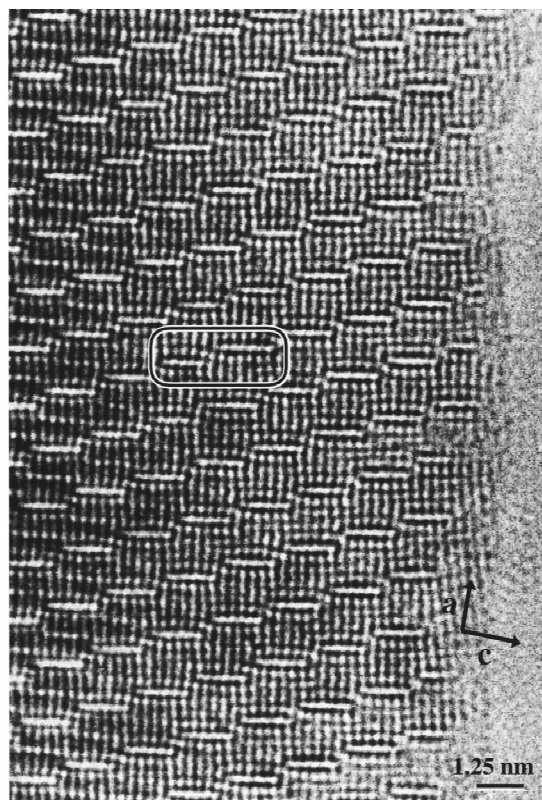
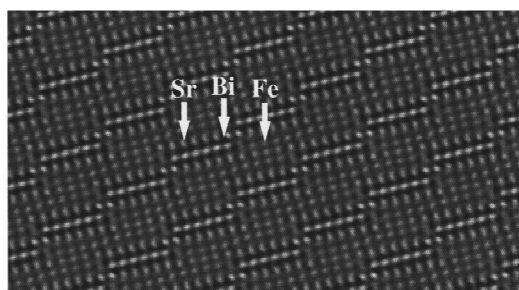


FIG. 8. Projection along $[010]$ of the accommodation zone outlining the part of Sr(3) atom in the bonding scheme. Only the O atoms bonded to Sr(3) and Fe(*e*) atoms are represented.



(a)



(b)

FIG. 9. (a) $[010]$ HREM image. The cation positions are imaged as dark dots. The framed area outlines a zone where the number of Bi atoms, within a ribbon, is varying. (b) Calculated image of a perfect structure with oval shaped ribbons 6 Bi wide. The contrast is the same as that of the experimental image. The crystal thickness is 15 Å and the focus value -260 Å (close to the Scherzer value). The nature of the cations is indicated.

unusual configuration as a result of its position between Fe(*a*) and two Sr(3) atoms (i.e., between the two 2_1 axes). These three differences give rise to the existence of “accommodation slices *E*” parallel to the (001) plane.

C. Nanostructure

An HREM study was performed on the powder samples and on the single crystal used for the present study.¹⁹ The contrast was interpreted using the simulated images calculated from the refined positional parameters (Table II). Different types of defects were characterized. No diffuse streaks were observed in the ED patterns, for the single crystal, in agreement with the x-ray observations. In the present

sample, the observed defects consist mainly in local variation of the contrast. An example of the [010] HREM image is given in Fig. 9(a), where the heavy electron density zones are imaged as dark dots. In the ideal structure, one observes double Bi ribbons which are 6 Bi wide [Fig. 9(b)]. In the experimental image, double Bi ribbons of variable lengths are observed (shown in Fig. 9). Such defects are expected to induce two effects: either the existence of supplementary Bi sites, with a partial occupancy, near both the Fe(*e*) and Sr(3) sites in coincidence with the bracketlike Bi ribbons longer than 6 Bi atoms, or the existence of supplementary partially occupied Sr and Fe sites near the Bi(*a*) and Bi(*f*) sites of the bracketlike Bi ribbons which are shorter than 6 Bi atoms. These defects are then likely to explain the difficulties encountered in determining both the positions and the occupancies of the atomic sites Fe(*e*), Sr(3), Bi(*a*), and Bi(*f*).

In the same way, contrast variations in the HREM images are observed near Bi(*a*). Such a feature was correlated to a local substitution of Fe for Bi on the Bi(*a*) site.¹⁹ The effect of these localized defects are visible mainly in the accommodation zones. In fact, they are likely to induce relatively large values for the thermal displacement parameters observed during the refinement. These values are the result of small displacements of the Bi atoms, depending on their relative location in the global Bi sequence, and are artificially increased by the existence of a static component.

As it is well known, there are strong correlations between the occupational and the thermal parameters. Coupled with the occurrence of many localized faults within the crystal, this prevents an accurate determination of the composition of the collapsed phase.

The relatively high value of the reliability factor $R = 0.069$ is likely to be related to the presence of the localized defects observed inside the crystal. Unfortunately, it is not possible to take into account such effects within an average model.

We obtained the chemical formula $\text{Bi}_{6.6}\text{Sr}_{8.4}\text{Fe}_5\text{O}_{26}$ instead of the ideal composition $\text{Bi}_6\text{Sr}_9\text{Fe}_5\text{O}_{26}$ when any substitution phenomenon is excluded. The electron probe microanalysis of some crystals leads to a Sr/Bi ratio equal to 1.33(8). This is close to the ratio $\text{Sr/Bi} = 1.27$ obtained for the chemical formula $\text{Bi}_{6.6}\text{Sr}_{8.4}\text{Fe}_5\text{O}_{26}$. The results for the iron atom are also in reasonable agreement with the composition refined from diffraction data.

V. CONCLUSION

Contrary to the related modulated structures, the collapsed phases described in the Bi-Sr-Cu-O and Bi-Sr-Ba-Cu-O systems have been well characterized by the usual three-

dimensional periodicity, but their structures were not yet clarified. The present study allows an accurate description of the original structure of the collapsed Bi-2212 phase $\text{Bi}_{6+x}\text{Sr}_{9-x}\text{Fe}_5\text{O}_{26}$ and a comparison with the incommensurate phase.

In contrast with the modulated compound, this phase exhibits mixed cation layers (Bi-Sr-Fe). The arrangement of the corresponding ribbons and the cation locations form atomic blocks (labeled *A*) which are also present in the Bi condensed regions of a half slab of the modulated phase. Two adjacent *A* blocks are shifted with respect to each other. Two supplementary Sr atoms, the common Fe(*a*)O₆ octahedra between the *A* blocks and the Bi(*a*) atoms in their intermediate configuration form an "accommodation slice *E*;" the mixed cation layers are then formed. The atomic *B* blocks, corresponding to the main disordered regions of the incommensurate phase, are missing in the collapsed compound, with the result that the corresponding structural static disorder does not appear in the collapsed phase where only localized disorders could be observed.

One can easily imagine that the structural features of the present collapsed phase also characterize the other known collapsed compounds and particularly those in the Bi-Sr-Cu-O system. These phases also present mixed cationic layers and their junction can be interpreted on the basis of the structural description of the "accommodation slice" of the present phase. The analogy both with the corresponding Bi-Sr-Ca-Cu-O and Bi-Sr-Fe-O modulated phases and with the collapsed Bi-Sr-Fe-O phase is a useful indication as to the actual structure of the Bi-Sr-Cu-O collapsed compounds. For example, the disordered region in the modulated compound $\text{Bi}_2\text{Sr}_2\text{CaCu}_2\text{O}_{8+\delta}$ (Ref. 2) is shorter than in the related iron phase, so the ordered Bi ribbons are longer. As expected, the observed Bi ribbons of the $\text{Bi}_{16}\text{Sr}_{28}\text{Cu}_{17}\text{O}_{69+\delta}$ (Ref. 5) collapsed phase are longer than in the $\text{Bi}_{6+x}\text{Sr}_{9-x}\text{Fe}_5\text{O}_{26}$ compound.

The main conclusion of the present study and of the previous studies of the Bi-Sr-Fe-O system is the existence of very close structural analogies between the Bi-Sr-(Ca)-Cu-O and the Bi-Sr-Fe-O systems and between the related modulated and collapsed phases. It emphasizes the interest in studying the iron phases which are more easily synthesized as single crystals and which allow a more accurate comprehension of the structural features of these phases.

ACKNOWLEDGMENTS

The authors are greatly indebted to Professor B. Raveau for encouragement and helpful discussions.

- ¹V. Petříček, Y. Gao, P. Lee, and P. Coppens, *Phys. Rev. B* **42**, 387 (1990).
- ²D. Grebille, H. Leligny, A. Ruyter, Ph. Labbé, and B. Raveau, *Acta Crystallogr. Sec. B* **52**, 628 (1996).
- ³M. Hervieu, C. Michel, A. Q. Pham, and B. Raveau, *J. Solid State Chem.* **104**, 289 (1993).
- ⁴M. Hervieu, C. Michel, M. T. Caldès, A. Q. Pham, and B.

Raveau, *J. Solid State Chem.* **107**, 117 (1993).

- ⁵M. Hervieu, M. T. Caldès, S. Cabrera, C. Michel, D. Pelloquin, and B. Raveau, *J. Solid State Chem.* **119**, 169 (1995).

- ⁶M. Hervieu, M. T. Caldès, C. Michel, D. Pelloquin, and B. Raveau, *J. Solid State Chem.* **118**, 357 (1995).

- ⁷M. Hervieu, D. Pelloquin, C. Michel, M. T. Caldès, and B. Raveau, *J. Solid State Chem.* **118**, 227 (1995).

- ⁸J. Darriet, F. Weill, B. Darriet, X. F. Zhang, and J. Etourneau, *Solid State Commun.* **86**, 227 (1993).
- ⁹O. Pérez, H. Leligny, D. Grebille, J. M. Grenêche, Ph. Labbé, D. Groult, and B. Raveau, *Phys. Rev. B* **55**, 1236 (1997).
- ¹⁰L. K. Templeton, *Acta Crystallogr.* **12**, 771 (1959).
- ¹¹Å. Kvik and M. Wulff, *Rev. Sci. Instrum.* **62**, 1073 (1992).
- ¹²J. P. Moy, A. P. Hammersley, S. O. Svensson, A. Thompson, K. Brown, L. Claustre, A. Gonzalez, and S. McSweeney, *J. Synchrotron. Radiat.* **3**, 1 (1996).
- ¹³A. P. Hammersley, computer code FIT2D v7.9, Experiments Division Programming Group, European Synchrotron Radiation Facility, Grenoble, France 1995.
- ¹⁴Z. Otwinowski, computer code DENZO, Science and Engineering Research Council/Daresbury Laboratory 1993.
- ¹⁵A. Altomare, M. C. Burla, M. Camalli, G. Cascarano, C. Giacovazzo, A. Guagliardi, and G. Polidori, *J. Appl. Crystallogr.* **27**, 435 (1994).
- ¹⁶Y. Lepage, W. R. McKinnon, J. M. Tarascon, and P. Barboux, *Phys. Rev. B* **40**, 6810 (1989).
- ¹⁷O. Pérez, H. Leligny, D. Grebille, Ph. Labbé, D. Groult, and B. Raveau, *J. Phys. C* **7**, 1003 (1995).
- ¹⁸V. Petříček, Crystallographic computing system SDS94, Institute of Physics, Academy of Sciences, Czech Republic, Prague, 1994.
- ¹⁹M. Hervieu, O. Pérez, D. Groult, D. Grebille, H. Leligny, and B. Raveau, *J. Solid State Chem.* **128**, (1997).